


ORIGINAL RESEARCH

Open Access



# Potential application of [ $^{18}\text{F}$ ]AIF-PSMA-11 PET/CT in radioiodine refractory thyroid carcinoma

Bliede Van den Broeck<sup>1\*</sup> , Jens M. Debacker<sup>2,3,4</sup>, Wouter Bauters<sup>5</sup>, David Creytens<sup>6,7</sup>, Liesbeth Ferdinande<sup>6,7</sup>, Wouter Huvenne<sup>4,8</sup>, Bruno Lapauw<sup>9,10</sup>, Vanessa Schelfhout<sup>7,11</sup>, Nick Van Laeken<sup>1</sup> and Charlotte Verroken<sup>9</sup>

## Abstract

**Background** Patients diagnosed with radioiodine refractory (RAI-R) thyroid carcinoma (TC) have a significantly worse prognosis than patients with radiosensitive TC. These refractory malignancies are often dedifferentiated, hindering the effectiveness of iodine-based imaging. Additionally, the role of metabolic imaging using [ $^{18}\text{F}$ ]FDG PET/CT is also limited in these cases, making adequate staging of RAI-R TC challenging. Recent case series have shown promising results regarding the role of the prostate-specific membrane antigen (PSMA) in TC. In this study we explored the value of [ $^{18}\text{F}$ ]AIF-PSMA-11 PET/CT in RAI-R TC.

**Methods** In this phase II study, lesions detected on [ $^{18}\text{F}$ ]AIF-PSMA-11 PET were compared to findings from [ $^{18}\text{F}$ ]FDG PET/CT. Additionally, the serologic soluble prostate-specific membrane antigen (sPSMA) was measured using ELISA. PSMA-expression on tumor tissue in any available resection specimens was analysed with an immunostainer.

**Results** Eight patients were included, with a total of 39 identified lesions based on PET imaging. [ $^{18}\text{F}$ ]AIF-PSMA-11 PET identified 30 of 39 lesions, and [ $^{18}\text{F}$ ]FDG PET identified 33 lesions, leading to a detection rate of 76.9% and 84.6%, respectively. Interestingly, while nine lesions were solely visualized on [ $^{18}\text{F}$ ]FDG, six were uniquely seen on [ $^{18}\text{F}$ ]AIF-PSMA-11 PET. While sPSMA was immeasurable in all female patients, no correlation was found between sPSMA in male patients and disease-related factors. In five out of eight patients immunohistology showed PSMA expression on the primary tumor.

**Conclusions** Although not all lesions could be visualized, [ $^{18}\text{F}$ ]PSMA-11 PET identified multiple lesions imperceptible on [ $^{18}\text{F}$ ]FDG PET. These results display the potential additional diagnostic role of PSMA-targeted imaging in patients with RAI-R TC.

*Trial registration number* No. EudraCT 2021-000456-19.

**Keywords** Thyroid carcinoma, Radio-iodine refractory thyroid carcinoma, PET/CT, PSMA-11

\*Correspondence:

Bliede Van den Broeck  
bliede.vandenbroeck@uzgent.be

Full list of author information is available at the end of the article



© The Author(s) 2024. **Open Access** This article is licensed under a Creative Commons Attribution-NonCommercial-NoDerivatives 4.0 International License, which permits any non-commercial use, sharing, distribution and reproduction in any medium or format, as long as you give appropriate credit to the original author(s) and the source, provide a link to the Creative Commons licence, and indicate if you modified the licensed material. You do not have permission under this licence to share adapted material derived from this article or parts of it. The images or other third party material in this article are included in the article's Creative Commons licence, unless indicated otherwise in a credit line to the material. If material is not included in the article's Creative Commons licence and your intended use is not permitted by statutory regulation or exceeds the permitted use, you will need to obtain permission directly from the copyright holder. To view a copy of this licence, visit <http://creativecommons.org/licenses/by-nc-nd/4.0/>.

## Background

Differentiated thyroid carcinoma (DTC) is a type of cancer derived from the follicular cells of the thyroid and is the most common type of thyroid carcinoma (TC) [1, 2]. Even in metastasized setting, DTC generally has a good prognosis, partly due to the therapeutic option of  $^{131}\text{I}$ , a well-tolerated and effective therapy [2, 3]. However, some patients present with tumors that do not or no longer respond to  $^{131}\text{I}$  therapy; this may result from impaired sodium iodide symporter expression as part of a dedifferentiation process [4]. Survival rates in radioiodine refractory (RAI-R) tumors are worse than in radioiodine-sensitive patients, particularly in those with metastatic disease [5–8]. To improve outcome, early detection of locoregional progressive or metastatic disease is essential. As in all DTC, serum thyroglobulin (Tg) is used as a tumor marker in patients with RAI-R TC. In addition, ultrasound and magnetic resonance imaging (MRI) are used for monitoring locoregional disease, and computed tomography (CT) and [ $^{18}\text{F}$ ]fluorodeoxyglucose ([ $^{18}\text{F}$ ]FDG) PET scans are used for the detection and monitoring of metastatic disease [3]. However, due to tumor dedifferentiation, Tg proves less representative as a tumor marker in RAI-R TC, and the current imaging techniques cannot always reveal the source of supposed disease recurrence or progression, displaying the need for new diagnostic tests.

Recently, novel radiotracers have been developed targeting the prostate-specific membrane antigen (PSMA), a marker of prostate epithelium that is overexpressed in prostate cancer cells. The implementation of PSMA-targeting agents has altered the role of nuclear medicine in the imaging and therapy of patients with prostate cancer [9–12]. However, contrary to what its name suggests, PSMA is not prostate-specific, as the protein is also expressed on cancer-induced neovasculature in other solid malignancies, including TC [13–17]. Multiple case reports have described an increased tracer uptake in incidental TC on PSMA PET [18–24]. Furthermore, histological overexpression of PSMA has been described in RAI-R DTC, in distant metastases and in poorly differentiated and undifferentiated TC [15, 25]. In addition, PSMA expression in the primary tumor has been described as a predictive factor for disease recurrence, tumor aggressiveness and RAI refractoriness [26, 27].

Some small studies have explored the role of PSMA PET in TC, but with various histologic subtypes and varying results [28–33]. The present study aimed to evaluate the use of PSMA-targeted PET as compared to [ $^{18}\text{F}$ ]FDG PET in a cohort of patients with RAI-R TC. Additionally, we examined the diagnostic significance of soluble serum PSMA (sPSMA) and the PSMA expression in available tumor resection specimens and biopsies.

## Materials and methods

### Patient inclusion

The current prospective study was designed as a cross-sectional, open-label phase 2b study in patients with RAI-R TC. The study was performed at a single tertiary referral center and approved by the local ethics committee and the competent authorities before study initiation (NCT05175404). Patients were eligible for the study when (1) they were diagnosed with histologically confirmed TC, with biochemical or iconographic evidence of persistent or recurrent disease, (2) the tumor was considered RAI-R according to European Thyroid Association guidelines [34], (3) female patients were either post-menopausal, surgically sterile, or used highly effective contraceptives and (4) all patients had to have had a routine clinical [ $^{18}\text{F}$ ]FDG PET/CT at most two months before inclusion. Exclusion criteria were (1) a known other active malignancy, (2) breastfeeding, or (3) being mentally or legally incapacitated. Between February and September 2022, 16 patients were considered eligible for inclusion of which eight agreed to participate in the study. There were no dropouts after inclusion. Information on sex, age, pathological tumor type and TNM classification [35], American Thyroid Association (ATA) risk score at diagnosis [3], and most recent unstimulated Tg level was recorded from the electronic patient files.

### [ $^{18}\text{F}$ ]AIF-PSMA-11 PET

The PSMA-tracer used in this study, [ $^{18}\text{F}$ ]AIF-PSMA-11, was produced in-house, as described elsewhere [36]. All patients received an [ $^{18}\text{F}$ ]AIF-PSMA-11 PET/CT, with an injected activity of  $2.0 \pm 0.2$  MBq/kg body weight. A PET scan was performed 60 min ( $\pm 5$  min) after tracer injection. PET imaging was preceded by a low-dose CT scan for attenuation correction and anatomical localization from the head to the mid-femoral region without administering intravenous contrast fluid. All [ $^{18}\text{F}$ ]AIF-PSMA-11 PET/CT scans were performed on a GE Discovery MI 3-ring PET scanner. The images were reconstructed using the QClear algorithm (GE Healthcare), a block sequential regularised expectation–maximization algorithm. Adverse events were monitored from the injection of the tracer until the patient left the nuclear medicine department.

### [ $^{18}\text{F}$ ]FDG PET/CT

All patients underwent [ $^{18}\text{F}$ ]FDG PET with diagnostic CT images in a routine clinical setting as part of the inclusion criteria. The scans were conducted in accordance with the EANM procedure guidelines for tumor imaging [37], covering the head to mid-femoral region, except for one patient who was scanned from head to feet, approximately 60 min after injection of a standard dose of [ $^{18}\text{F}$ ]

FDG (3.7 MBq per kg body weight + 37 MBq). A diagnostic CT was performed as part of the [ $^{18}\text{F}$ ]FDG PET/CT scan. In six out of eight patients intravenous contrast was administered.

### Image analysis

All analyses on PET images were performed using Oasis software (Segami corp., Columbia, USA) on AGFA Impax (AGFA Healthcare, Mortsel, Belgium). All PET images were analyzed by a certified nuclear medicine physician with experience in reading [ $^{18}\text{F}$ ]FDG and [ $^{18}\text{F}$ ]AIF-PSMA-11 PET and were assessed for the presence of any lesions and their location. All CT images were analyzed by a certified radiologist with experience in head and neck imaging. Diagnostic CT images from the [ $^{18}\text{F}$ ]FDG PET/CT were used to correlate the findings on both [ $^{18}\text{F}$ ]AIF-PSMA-11 PET and [ $^{18}\text{F}$ ]FDG PET to accurately distinguish between suspicious lesions in the context of thyroid cancer and benign lesions or sites of normal physiological uptake such as degenerative bone lesions or urinary excretion. The CT images were also used to identify any suspicious lesion that would be negative on both [ $^{18}\text{F}$ ]AIF-PSMA-11 PET and [ $^{18}\text{F}$ ]FDG PET.

The number of lesions delineated in each organ was limited to 10 on each PET. For each lesion, the maximal standard uptake value (SUV),  $\text{SUV}_{\text{max}}$ , and metabolic tumor volume (MTV) were determined using a margin threshold set at 41% of the  $\text{SUV}_{\text{peak}}$  value. If needed, a manual adjustment of the delineation was made, for example, to exclude physiologic uptake in an adjacent region. Additionally, background  $\text{SUV}_{\text{mean}}$  values were determined in the parotid glands, the mediastinal blood pool, and the liver. Dimensions on CT were measured along the short axial axis for lymph nodes and along the long axis for all other lesions. Hounsfield Units were measured on the CT without contrast of the PSMA PET scan.

### sPSMA measurements

Before injection of the radiolabelled PSMA, a venous blood sample was taken from all patients. All samples were collected, centrifuged, and stored for batch processing. An enzyme-linked immunosorbent assay (ELISA; Assay Genie, Dublin, Ireland) was used to analyze sPSMA [38]. All measurements were made in duplicate and according to the manufacturer's specifications. Intra-assay coefficient of variation was 5.36%, lower limit of quantification was 2.81 ng/mL.

### Histology

For each case, 4- $\mu\text{m}$ -thick sections from representative blocks of formalin-fixed, paraffin-embedded tumor tissue were used for immunohistochemical analysis.

Immunohistochemistry was performed using an immunostainer (Benchmark XT, Ventana Medical Systems, Tucson, AZ, USA), according to the manufacturer's instructions. The sections were immunostained with a primary monoclonal antibody against PSMA (1:25; EP192; Cell Marque). Visualization was achieved with ultraView Universal DAB Detection kit (Ventana Medical Systems, Tucson, AZ, USA). Appropriate positive and negative controls were used throughout the study. PSMA expression was evaluated by two expert pathologists on immunostained whole tissue sections (Olympus, BX53; 40 $\times$  magnification). The 3-point PSMA scale proposed by Bychkov et al. was used to score PSMA positivity [39]: no detectable endothelial expression or expression in <5% of capillaries was defined as negative (score 0), PSMA expression in 6–50% of capillaries as moderately positive (score 1) and PSMA expression in >50% of capillaries as strongly positive (score 2). PSMA expression was evaluated on the primary tumor in all eight patients and in available metastatic lesions in five patients, consisting of two bone metastases, one brain metastasis and two lung metastases.

### Statistics

Descriptive statistics are expressed as mean  $\pm$  standard deviation (SD) or median (range). The amount, type,  $\text{SUV}_{\text{max}}$ , and MTV of lesions on [ $^{18}\text{F}$ ]AIF-PSMA-11 PET were compared with the [ $^{18}\text{F}$ ]FDG PET using both a lesion-based and a patient-based approach. Detection rates were calculated for both [ $^{18}\text{F}$ ]AIF-PSMA-11 PET and [ $^{18}\text{F}$ ]FDG PET. The total number of suspicious lesions was defined as all suspicious lesions visible on [ $^{18}\text{F}$ ]AIF-PSMA-11 PET, [ $^{18}\text{F}$ ]FDG PET and/or CT. Spearman correlation coefficients were used to evaluate associations between semi-quantitative parameters on [ $^{18}\text{F}$ ]AIF-PSMA-11 and [ $^{18}\text{F}$ ]FDG PET, serological markers including unstimulated Tg levels and sPSMA, and immunohistochemistry results. All statistical analyses were performed using SPSS Statistics 28 (IBM, New York, USA), and  $p < 0.05$  was considered statistically significant.

## Results

### Patient characteristics

Eight patients (four male, four female) were included in this study, with a mean age of 66 years ( $\pm 7$  years). The included patients were diagnosed with follicular TC ( $n=4$ ), papillary TC ( $n=2$ ), follicular variant of papillary TC ( $n=1$ ) or poorly differentiated TC ( $n=1$ ). At the time of initial diagnosis (between 1988 and 2022), five patients had a high ATA risk score, one had an intermediate ATA risk score, and two had a low ATA risk score. The included patients were considered iodine refractory based on the absence of uptake of RAI in all ( $n=2$ ) or

some (n=1) lesions on a post-therapy scan, absence of uptake of RAI in all lesions on a diagnostic iodine scan (n=3), progressive disease 6 months after treatment with RAI (n=1), or persistent disease despite treatment with maximal dose of RAI (n=1; cumulative dose 950 mCi). Seven patients were previously treated with RAI, with cumulative activities ranging from 100 to 950 mCi. Two patients were treated with a tyrosine kinase inhibitor at the time of inclusion (PT3: lenvatinib 10 mg and PT7: lenvatinib 14 mg). PT3 had previously been treated with sorafenib 200 mg but this treatment was discontinued due to intolerance. The most recent unstimulated Tg levels ranged from 1.13 µg/dl to 2270 µg/dl with a median of 132.25 µg/dl; none of the patients had Tg antibodies. An overview of the patient characteristics can be found in Table 1.

**[18F]AIF-PSMA-11 PET**

The mean administered activity of [18F]AIF-PSMA-11 was 143.30 MBq (+/-23.7 MBq). The time between tracer injection and start of the PET scan was exactly 60 min for each patient. The median time between the [18F]FDG PET and [18F]AIF-PSMA-11 PET was 4 days (range 2–35 days). No adverse events were recorded.

Background SUV<sub>mean</sub> in the liver on [18F]AIF-PSMA-11 PET has a median of 4,6 but with a wide range from 1.9 to 12.9. The mean background SUV<sub>mean</sub> in the parotid gland was 9.0 (+/-0.9), excluding two patients with bilateral parotid atrophy and, as such, no uptake of PSMA. The mean SUV<sub>mean</sub> in the mediastinal blood pool was 1.1 (+/-0.2).

For the lesion-based analysis, a total of 30 suspicious lesions were identified on [18F]AIF-PSMA-11 PET with a median SUV<sub>max</sub> of 4.0 (range 1.2–14.8). On [18F]FDG PET, 33 lesions were found with a median SUV<sub>max</sub> of 5.3 (range 2.3–44.9). In total, there were 39

lesions on [18F]AIF-PSMA-11 and [18F]FDG PET combined. No additional suspicious lesions were visualized on the CT part of the [18F]FDG PET/CT. These results provide a detection rate of 76.9% for [18F]AIF-PSMA-11 PET and a detection rate of 84.6% for [18F]FDG PET. Twenty-four lesions were visible on both [18F]AIF-PSMA-11 PET and [18F]FDG PET, including one locoregional recurrence, one lymph node, ten bone lesions and twelve lung lesions. Six lesions in five patients were only visible on [18F]AIF-PSMA-11 PET, of which two were located in the brain, one was a local recurrence, one was a lymph node, and two were bone lesions. Nine lesions in three patients were only visible on [18F]FDG PET, consisting of eight lung lesions and one lymph node (Fig. 1). Further characteristics, including lesion size and Hounsfield units on non-contrast enhanced CT, can be found in Table 2. In one patient with papillary TC, the only visible lesion was an FDG-positive, PSMA-negative lymph node; in another patient with follicular TC, the only lesion was a PSMA-positive, FDG-negative brain metastasis. Interestingly, a combination of both PSMA-positive, FDG-negative lesions and PSMA-negative, FDG-positive lesions was observed in one patient with follicular TC.

On a patient-based analysis, the median of the mean SUV<sub>max</sub> of all lesions per patient was 10.34 (range 0–11.21) on [18F]AIF-PSMA-11 PET and 3.70 (range 0–20.72) on [18F]FDG PET. An overview of the patient-based analysis can be found in Table 3. Statistical analysis showed a significant correlation between total metabolic tumor volume (TMTV) of the lesions on [18F]PSMA and [18F]FDG PET (r(8)=0.987; p<0.001), as well as between TMTV on [18F]PSMA PET and thyroglobulin levels (r(8)=0.852; p=0.007) and between TMTV on [18F]FDG PET and thyroglobulin levels (r(8)=0.912; p=0.002).

**Table 1** Overview of patient characteristics

	Gender	Age	Histology	Primary diagnosis	ATA risk score	TNM staging *	Unstimulated Tg (µg/dl)	Cumulative <sup>131</sup> I activity (mCi)**
PT1	Male	75	Papillary, follicular variant	2009	High	T1bN0M1	234	950 (150+200+200+200+200)
PT2	Female	70	Follicular	1994	Low	T2NXMX	8.03	200
PT3	Female	56	Follicular	2007	Low	T3aN0M0	245	100
PT4	Female	63	Follicular	2016	High	T3aN1M1	23.5	100
PT5	Male	63	Papillary	1988	High	T1aN1M1	1.13	500 (100+100+150+150)
PT6	Male	69	Papillary	2009	Intermediate	T2N1M0	53.5	350 (100+100+150)
PT7	Female	59	Follicular	2014	High	T4aN1M1	211	400 (100+100+200)
PT8	Male	74	Poorly differentiated	2022	High	T4aN0M1	2270	0

ATA American Thyroid Association; Tg thyroglobulin

\* According to TNM classification of malignant tumours, eighth edition

\*\* Between brackets: activities of each separate <sup>131</sup>I treatment



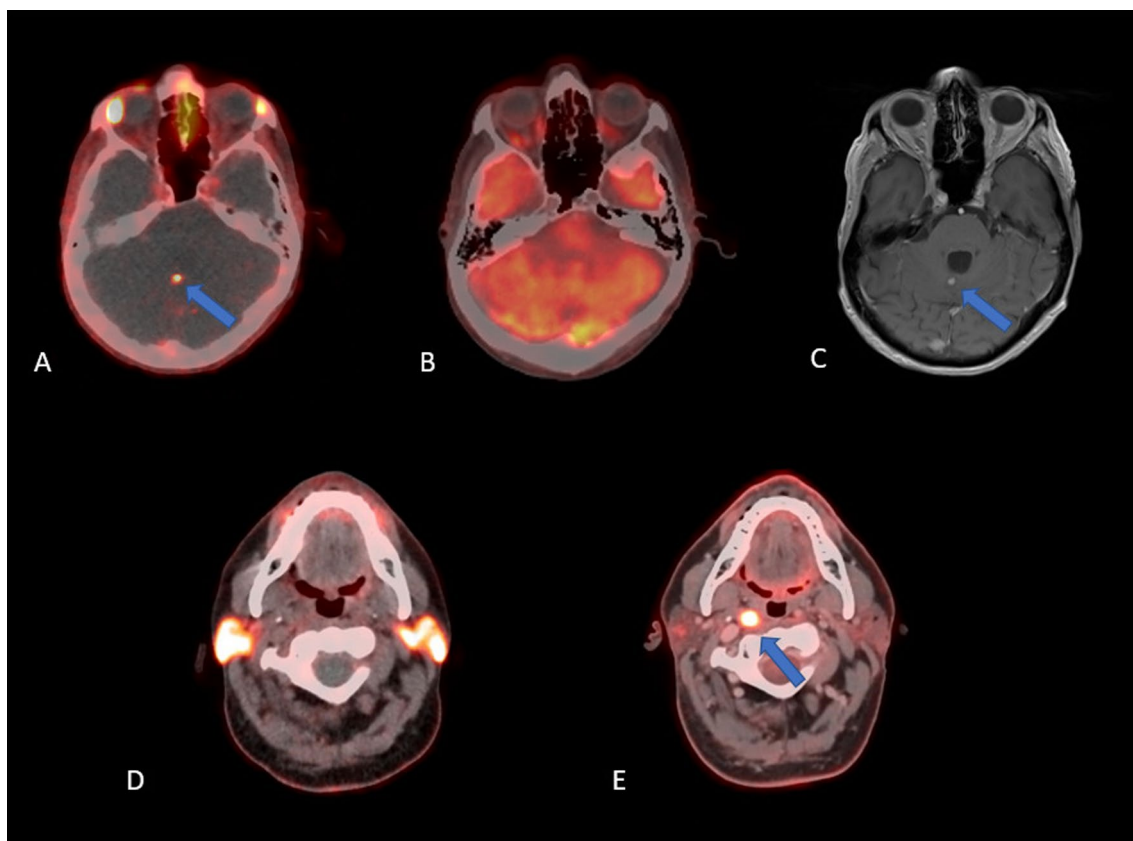


**Fig. 1** Example of a lesion that is only visible on PSMA PET (PT1) and a lesion that is only visible on FDG PET (PT 6). **A** PSMA PET/CT axial fusion images. **B** FDG PET/CT axial fusion images. **C** T1 weighted MRI images with gadolinium. **D** PSMA PET/CT axial fusion images. **E** FDG PET/CT axial fusion images; **A–C** shows focal uptake in the cerebellum on PSMA PET (blue arrow), not visible on FDG PET, corresponding with a known metastasis on MRI; **D, E** shows intense focal uptake on FDG PET, without uptake on PSMA PET in a known pathologic retropharyngeal lymph node

### sPSMA

sPSMA levels were measurable in the four male patients with a mean of  $37.7 \pm 17.56$  ng/mL (range 20.3–55.9). The four female patients had undetectable sPSMA levels. Correlation analysis showed no significant correlations between sPSMA and TMTV or mean  $SUV_{max}$  on PSMA or FDG PET nor between sPSMA and Tg levels.

### Histology

Immunostaining proved positive in five of the primary TC (PT1, PT2, PT3, PT7 and PT8) (63%) and negative in the remaining three (PT4, PT5 and PT6) (37%). Among the five positive cases, PSMA expression was scored moderately positive (score 1) in three cases (PT1, PT2 and PT3) and strongly positive (score 2) in two cases (PT7 and PT8). Endothelial expression of PSMA was exclusively localized within tumor tissue, but not in normal or non-neoplastic thyroid tissue. There were no significant correlations between the PSMA-score in the primary tumor and any parameters on either PSMA or FDG PET, or sPSMA levels.

Of the three patients without PSMA expression on the primary tumor, PT4 and PT5 did have PSMA-positive lesions at 6 years and 34 years after diagnosis. The third patient, PT6 had one FDG-positive lesion, but without PSMA-uptake.

Positive PSMA endothelial expression was observed in all five histologically examined metastases: strong (score 2) expression in 2 bone metastases (PT1 and PT8) and one brain metastasis (PT7) (Fig. 2), moderate (score 1) expression in 2 lung metastases (PT2 and PT3). No metastatic tissue samples were available for immunostaining of the patients that had no PSMA-expression on the primary tumor.

### Discussion

The current study aimed to assess the performance of [ $^{18}\text{F}$ ]AIF-PSMA-11 PET compared to [ $^{18}\text{F}$ ]FDG PET in a homogeneous cohort of patients with RAI-R TC. A total of 39 lesions were identified as suspicious in the cohort of included patients. Of these, [ $^{18}\text{F}$ ]AIF-PSMA-11 PET detected 30 lesions, whereas [ $^{18}\text{F}$ ]FDG PET detected 33

**Table 2** Lesion characteristics on PSMA and FDG PET

	Patient	Type	PSMA SUVmax	PSMA MTV (ml)	FDG SUVmax	FDG MTV (ml)	Lesion size (mm)	Hounsfield units
Lesion 1	PT1	Brain	8.8	0.44	ND	0	ND	ND
Lesion 2	PT1	Bone	10.1	53.46	5.0	30.04	370	147
Lesion 3	PT1	Bone	14.8	2.72	3.8	0.87	ND	ND
Lesion 4	PT2	Local	9.1	3.30	ND	0	ND	ND
Lesion 5	PT2	Lung	6.3	7.57	6.1	6.15	17	66
Lesion 6	PT2	Lung	2.6	2.85	3.8	2.93	19	55
Lesion 7	PT2	Lung	2.3	3.10	3.4	3.1	13	34
Lesion 8	PT2	Lung	ND	0	5.8	2.66	49	41
Lesion 9	PT2	Lung	ND	0	4.6	2.49	17	33
Lesion 10	PT2	Lung	2.3	7.55	5.3	8.06	21	39
Lesion 11	PT2	Lung	2.9	5.11	2.5	5.76	9	4
Lesion 12	PT2	Lung	3.5	6.32	3.3	5.67	11	25
Lesion 13	PT2	Lung	4	53.83	8.4	54.33	16	35
Lesion 14	PT2	Lung	4.6	5.13	4.3	9.35	23	57
Lesion 15	PT2	Bone	3.9	4.14	6.6	5.07	16	47
Lesion 16	PT2	Bone	7	47.39	4	26.34	38	44
Lesion 17	PT3	Lung	ND	0	14.6	0.96	4	-5
Lesion 18	PT3	Lung	ND	0	30.9	0.87	8	34
Lesion 19	PT3	Lung	4.2	5.26	44.9	6.30	21	41
Lesion 20	PT3	Lung	ND	0	6.2	2.24	5	19
Lesion 21	PT3	Lung	ND	0	2.3	0.10	3	-256
Lesion 22	PT3	Lung	ND	0	14.1	2.12	7	32
Lesion 23	PT3	Lung	2	1.87	29.5	1.93	8	34
Lesion 24	PT3	Lung	2.1	1.52	24.7	0.85	7	-95
Lesion 25	PT3	Lung	ND	0	9.8	1.31	6	15
Lesion 26	PT3	Lung	4.1	7.71	30.2	6.26	18	48
Lesion 27	PT4	Local	2.3	0.77	4.8	0.81	11	85
Lesion 28	PT4	Bone	7.5	2.68	7.2	1.89	5	168
Lesion 29	PT4	Bone	3.6	0.87	5.3	1.35	9	93
Lesion 30	PT5	Lymph node	2	0.89	2.3	0.46	10	22
Lesion 31	PT5	Lymph node	2.3	0.37	ND	0	8	8
Lesion 32	PT6	Lymph node	ND	0	24.3	0.80	7	50
Lesion 33	PT7	Brain	4.3	3.76	ND	0	21	38
Lesion 34	PT8	Bone	4.2	3.91	ND	0	12	305
Lesion 35	PT8	Bone	3.1	0.77	ND	0	ND	ND
Lesion 36	PT8	Bone	4.5	13.74	4.4	6.87	32	66
Lesion 37	PT8	Bone	5.2	10.91	4.2	7.96	18	73
Lesion 38	PT8	Bone	3.7	6.55	2.5	8.16	20	23
Lesion 39	PT8	Bone	2.9	247	4.7	324	105	36

ND not detectable

lesions. As such, the detection rate of [<sup>18</sup>F]AIF-PSMA-11 PET was 76.9%, lower than the 84.6% with the current gold standard of [<sup>18</sup>F]FDG PET. However, despite the higher number and mean tracer uptake of lesions detected by [<sup>18</sup>F]FDG PET, [<sup>18</sup>F]AIF-PSMA-11 PET was able to detect 6 lesions that were not detected by [<sup>18</sup>F]FDG PET. Furthermore, in one out of eight patients,

disease localization was achieved only by [<sup>18</sup>F]AIF-PSMA-11 PET. Our results are consistent with previous studies in DTC which also found a lower detection rate in [<sup>68</sup>Ga]Ga-PSMA-11 and [<sup>68</sup>Ga]Ga-HBED-CC-PSMA PET compared with [<sup>18</sup>F]FDG PET and in line with the study from Shi et al., which also included also a patient group with RAI-R DTC [28–30, 40].

**Table 3** Patient-based analysis of PSMA and FDG PET, sPSMA and immunohistochemistry

	Lesions PSMA	Mean SUVmax PSMA	TMTV PSMA (ml)	Lesions FDG	Mean SUVmax FDG	TMTV FDG (ml)	Lesions total	sPSMA (ng/ml)	Histology score (primary tumor)
PT1	3	11.21	56.62	2	2.92	30.91	3	25.28	1
PT2	11	3.73	146.29	12	4.47	131.91	13	ND	1
PT3	4	1.24	16.36	10	20.72	22.94	10	ND	1
PT4	3	4.47	4.32	3	5.77	4.05	3	ND	0
PT5	2	2.15	1.26	1	1.15	0.46	2	49.43	0
PT6	0	0	0	1	24.3	0.8	1	20.32	0
PT7	1	4.3	3.76	0	0	0	1	ND	2
PT8	6	3.93	282.88	4	2.63	346.99	6	55.89	2

TMTV total metabolic tumor volume; ND not detectable

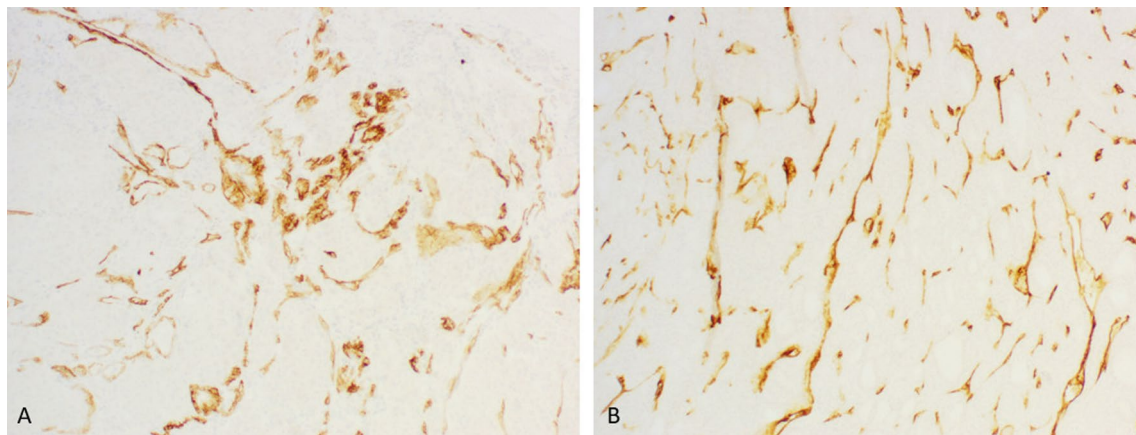


**Fig. 2** Example of strong PSMA expression in a primary tumor (PT8) and in a brain metastasis (PT7). **A** Strong PSMA expression (score 2) in thyroid resection specimen of poorly differentiated TC. **B** Strong PSMA expression (score 2) in brain metastasis of a follicular TC

Interestingly, we observed a distinction between the types of lesions detectable by both PET modalities. Generally, more bone lesions were visible on  $[^{18}\text{F}]\text{AIF-PSMA-11}$  PET compared to  $[^{18}\text{F}]\text{FDG}$  PET, while the inverse was true for lung metastases. Furthermore, the two brain metastases were only detectable using  $[^{18}\text{F}]\text{AIF-PSMA-11}$  PET. Various factors could account for these observations. First, the high background activity of  $[^{18}\text{F}]\text{FDG}$  in the brain may account for the discrepancies between  $[^{18}\text{F}]\text{FDG}$  PET and  $[^{18}\text{F}]\text{AIF-PSMA-11}$  PET in detecting brain metastases. Second, the visualisation of bone metastases on  $[^{18}\text{F}]\text{AIF-PSMA-11}$  PET might be partly attributable to the fluor element rather than the PSMA moiety of the tracer. Indeed,  $^{18}\text{F}$ -labeled PSMA tracers are known for their higher skeletal uptake, including bone metastases and benign bone lesions, compared to their  $^{68}\text{Ga}$ -labeled counterparts [41–43]. Third, although angiogenesis is a hallmark of cancer, there have been speculations that not all cancer cells induce new blood vessel formation for their vascularisation but that

some could utilize pre-existing blood vessels as a form of vessel co-option [44, 45]. Vessel co-option could be a common characteristic of lung metastases and a mode of resistance to anti-angiogenic therapy [44–48]. As for now, the occurrence of vessel co-option in TC metastases has not been examined yet. Since PSMA expression is only observed on the endothelial cells of the newly formed and not on normal vascular endothelial cells, vessel co-option might account for why lung metastases exhibit lower uptake in  $[^{18}\text{F}]\text{PSMA}$  PET scan.

Taken together, PSMA and FDG PET seem to visualize different facets of the oncologic process, tumor glucose metabolism and neovascularization, suggesting that PSMA PET may complement FDG PET in the diagnosis and follow-up of RAI-R TC. For example, PSMA PET could assist in detecting the origin of an increasing tumor marker when standard imaging techniques are unsuccessful.

Remarkably, two patients without PSMA expression on the primary tumor had PSMA-positive lesions 6 and

34 years after resection of the primary tumor, suggesting that PSMA expression could be variable at one time point or may emerge progressively over time. Therefore, both our imaging and histology results may reflect tumoral heterogeneity.

In addition to the potential use of targeting PSMA using PET imaging, we also evaluated the value of measuring sPSMA in patients with RAI-R TC. We hypothesized that an increase in neovasculature formation could impact the amount of protein shed from the tumor, which could be a potential biomarker for tumor growth. However, in this small cohort, sPSMA was only detectable in male patients and showed no correlation with any of the FDG or PSMA PET parameters, while sPSMA remained below the detection limit in all female patients. Probably, rather than being a potential tumor marker, sPSMA seems to reflect the presence of prostate tissue.

In this proof-of-concept study, we aimed to evaluate the role of PSMA as a biomarker in RAI-R TC, by means of [<sup>18</sup>F]PSMA PET, sPSMA and immunohistology in a cohort of patients with RAI-R TC. However some limitations need to be acknowledged. The first limitation is the lack of histological confirmation for lesions that showed discrepancies between [<sup>18</sup>F]AIF-PSMA-11 and [<sup>18</sup>F]FDG PET results. Most of these lesions were already confirmed sites of disease recurrence or metastases, but some, such as bone lesions, were not previously identified. However, due to the invasive nature of biopsies, histological confirmation of previously unknown lesions was not part of this study. An important second limitation in this study is the small sample size. Even though this study was conducted in a tertiary reference center, only a few patients met the inclusion criteria and were included.

Nevertheless, the results of this small cohort corroborate the potential value of targeting PSMA in this relatively rare group of patients. Our findings do not provide conclusive results, so more in-depth research is necessary to develop a more nuanced understanding of the use of PSMA PET in the diagnosis and staging of RAI-R TC. Future studies should aim to include larger patient cohorts and address the limitations identified in our current work, thereby ensuring more generalizable results.

## Conclusion

[<sup>18</sup>F]AIF-PSMA-11 PET imaging demonstrates encouraging results in patients with RAI-R TC. [<sup>18</sup>F]AIF-PSMA-11 PET detected six lesions that were not visible on [<sup>18</sup>F]FDG PET, including a solitary lesion in one patient. These discrepancies indicate a potential role for PSMA-targeted PET imaging in patients with RAI-R TC when other imaging techniques, including [<sup>18</sup>F]FDG PET fail to locate the source of disease progression. While larger prospective studies are required,

these results add to the existing pool of data that may suggest an additional role for PSMA PET in thyroid carcinoma.

## Abbreviations

ATA	American Thyroid Association
CT	Computed tomography
DTC	Differentiated thyroid carcinoma
FDG	Fluorodeoxyglucose
MRI	Magnetic resonance imaging
MTV	Metabolic tumor volume
PET	Positron emission tomography
PSMA	Prostate-specific membrane antigen
RAI-R	Radioiodine refractory
sPSMA	Serologic soluble prostate-specific membrane antigen
SD	Standard deviation
SUV	Standard uptake value
TC	Thyroid carcinoma
Tg	Thyroglobulin
TMTV	Total metabolic tumor volume

## Acknowledgements

The authors want to thank the nuclear medicine and radiopharmacy team for their contributions to the scanning and the production of F-PSMA-11.

## Author contributions

Study concept and design: BVDB, JMD, DC, LF, WH, BL, VS, CV. Data collection: BVDB, WB, DC, LF, BL, NVL, CV. Analysis and interpretation of data: BVDB, DC, LF, BL, VS, CV. Drafting of the manuscript: all authors. Revision of the manuscript: all authors. All authors read and approved the final manuscript.

## Funding

A grant was received from CRIG (Cancer Research Institute Ghent).

## Availability of data and materials

The datasets used and/or analysed during the current study are available from the corresponding author on reasonable request.

## Declarations

### Ethics approval and consent to participate

This study was approved by the local ethics committee of the university hospital Ghent and the competent authorities before study initiation (NCT05175404). This study was performed in accordance with the ethical standards as laid down in the 1964 Declaration of Helsinki and its later amendments or comparable ethical standards.

A written informed consent was obtained from all participants.

### Consent for publication

Not applicable.

### Competing interests

No conflict of interest.

### Author details

<sup>1</sup>Department of Medical Imaging, Nuclear Medicine, Ghent University Hospital, C. Heymanslaan 10, 9000 Ghent, Belgium. <sup>2</sup>Molecular Imaging and Therapy Research Group (MITH), Vrije Universiteit Brussel (VUB), Brussels, Belgium.

<sup>3</sup>Department of Nuclear Medicine, Vrije Universiteit Brussel (VUB), Universitair Ziekenhuis Brussel (UZ Brussel), Brussels, Belgium. <sup>4</sup>Department of Head and Neck Surgery, Ghent University Hospital, Ghent, Belgium. <sup>5</sup>Department of Medical Imaging, Radiology, Ghent University Hospital, Ghent, Belgium. <sup>6</sup>Department of Pathology, Ghent University Hospital, Ghent, Belgium. <sup>7</sup>Department of Diagnostic Sciences, Ghent University, Ghent, Belgium. <sup>8</sup>Department of Head and Neck Surgery, Ghent University Hospital, Ghent, Belgium. <sup>9</sup>Department of Endocrinology, Ghent University Hospital, Ghent, Belgium. <sup>10</sup>Department of Internal Medicine and Pediatrics, Ghent University, Ghent, Belgium. <sup>11</sup>Department of Nuclear Medicine, AZ Sint-Jan Brugge, Brugge, Belgium.



Received: 19 April 2024 Accepted: 29 August 2024  
Published online: 12 September 2024

## References

- Lim H, Devesa SS, Sosa JA, Check D, Kitahara CM. Trends in thyroid cancer incidence and mortality in the United States, 1974–2013. *JAMA*. 2017;317:1338–48.
- Paschke R, Lincke T, Müller SP, Kreissl MC, Dralle H, Fassnacht M. The treatment of well-differentiated thyroid carcinoma. *Dtsch Arztebl Int*. 2015;112:452–8.
- Haugen BR, Alexander EK, Bible KC, Doherty GM, Mandel SJ, Nikiforov YE, et al. 2015 American Thyroid Association management guidelines for adult patients with thyroid nodules and differentiated thyroid cancer: The American Thyroid Association guidelines task force on thyroid nodules and differentiated thyroid cancer. *Thyroid*. 2016;26:1–133.
- Liu J, Liu Y, Lin Y, Liang J. Radioactive iodine-refractory differentiated thyroid cancer and redifferentiation therapy. *Endocrinol Metab*. 2019;34:215–25.
- Cabanillas ME, Patel A, Danysh BP, Dadu R, Kopetz S, Falchook G. BRAF inhibitors: experience in thyroid cancer and general review of toxicity. *Horm Cancer*. 2015;6:21–36.
- Babu G, Kainickal CT. Update on the systemic management of radioactive iodine refractory differentiated thyroid cancer (review). *Mol Clin Oncol*. 2021;14:35.
- Durante C, Haddy N, Baudin E, Leboulleux S, Hartl D, Travagli JP, et al. Long-term outcome of 444 patients with distant metastases from papillary and follicular thyroid carcinoma: benefits and limits of radioiodine therapy. *J Clin Endocrinol Metab*. 2006;91:2892–9.
- Worden F. Treatment strategies for radioactive iodine-refractory differentiated thyroid cancer. *Ther Adv Med Oncol*. 2014;6:267–79.
- Maurer T, Eiber M, Schwaiger M, Gschwend JE. Current use of PSMA-PET in prostate cancer management. *Nat Rev Urol*. 2016;13:226–35.
- Bouchelouche K, Choyke PL. Advances in prostate-specific membrane antigen PET of prostate cancer. *Curr Opin Oncol*. 2018;30:189–96.
- Farolfi A, Calderoni L, Mattana F, Mei R, Telo S, Fanti S, et al. Current and emerging clinical applications of PSMA PET diagnostic imaging for prostate cancer. *J Nucl Med Off Publ Soc Nucl Med*. 2021;62:596–604.
- Hofman MS, Violet J, Hicks RJ, Ferdinandus J, Thang SP, Akhurst T, et al. [177Lu]-PSMA-617 radionuclide treatment in patients with metastatic castration-resistant prostate cancer (LuPSMA trial): a single-centre, single-arm, phase 2 study. *Lancet Oncol*. 2018;19:825–33.
- Kinoshita Y, Kuratsukuri K, Landas S, Imaida K, Rovito PM, Wang CY, et al. Expression of prostate-specific membrane antigen in normal and malignant human tissues. *World J Surg*. 2006;30:628–36.
- Silver DA, Pellicer I, Fair WR, Heston WD, Cordon-Cardo C. Prostate-specific membrane antigen expression in normal and malignant human tissues. *Clin Cancer Res Off J Am Assoc Cancer Res*. 1997;3:81–5.
- Heitkötter B, Steinestel K, Trautmann M, Grünwald I, Barth P, Gevensleben H, et al. Neovascular PSMA expression is a common feature in malignant neoplasms of the thyroid. *Oncotarget*. 2018;9:9867–74.
- Haffner MC, Kronberger IE, Ross JS, Sheehan CE, Zitt M, Mühlmann G, et al. Prostate-specific membrane antigen expression in the neovascularity of gastric and colorectal cancers. *Hum Pathol*. 2009;40:1754–61.
- Chang SS, Reuter VE, Heston WD, Bander NH, Grauer LS, Gaudin PB. Five different anti-prostate-specific membrane antigen (PSMA) antibodies confirm PSMA expression in tumor-associated neovascularity. *Cancer Res*. 1999;59:3192–8.
- Sager S, Vatankulu B, Uslu L, Sönmezoglu K. Incidental detection of follicular thyroid carcinoma in 68Ga-PSMA PET/CT imaging. *J Nucl Med Technol*. 2016;44:199–200.
- Tang K, Wang Z, Lin J, Zheng X. Hürthle cell thyroid adenoma showing avid uptake on 18F-PSMA-1007 PET/CT. *Clin Nucl Med*. 2020;45:223–4.
- Ciappuccini R, Edet-Sanson A, Saguet-Rysanek V, Gauthé M, Bardet S. Thyroid incidentaloma on 18F-fluorocholine PET/CT and 68Ga-PSMA PET/CT revealing a medullary thyroid carcinoma. *Clin Nucl Med*. 2019;44:663–5.
- Derlin T, Kreipe H-H, Schumacher U, Soudah B. PSMA expression in tumor neovascularity endothelial cells of follicular thyroid adenoma as identified by molecular imaging using 68Ga-PSMA ligand PET/CT. *Clin Nucl Med*. 2017;42:e173–4.
- Damle NA, Bal C, Singh TP, Gupta R, Reddy S, Kumar R, et al. Anaplastic thyroid carcinoma on 68 Ga-PSMA PET/CT: opening new frontiers. *Eur J Nucl Med Mol Imaging*. 2018;45:667–8.
- Taywade SK, Damle NA, Bal C. PSMA expression in papillary thyroid carcinoma: opening a new horizon in management of thyroid cancer? *Clin Nucl Med*. 2016;41:e263–265.
- Verburg FA, Krohn T, Heinzl A, Mottaghy FM, Behrendt FF. First evidence of PSMA expression in differentiated thyroid cancer using [<sup>68</sup>Ga]PSMA-HBED-CC PET/CT. *Eur J Nucl Med Mol Imaging*. 2015;42:1622–3.
- Moore M, Panjwani S, Mathew R, Crowley M, Liu Y-F, Aronova A, et al. Well-differentiated thyroid cancer neovascularity expresses prostate-specific membrane antigen—a possible novel therapeutic target. *Endocr Pathol*. 2017;28:339–44.
- Sollini M, di Tommaso L, Kirienco M, Piombo C, Erreni M, Lania AG, et al. PSMA expression level predicts differentiated thyroid cancer aggressiveness and patient outcome. *EJNMMI Res*. 2019;9:93.
- Ryu YJ, Lim SY, Na YM, Park MH, Kwon SY, Lee JS. Prostate-specific membrane antigen expression predicts recurrence of papillary thyroid carcinoma after total thyroidectomy. *BMC Cancer*. 2022;22:1278.
- Lütje S, Gomez B, Cohnen J, Umutlu L, Gotthardt M, Poeppel TD, et al. Imaging of prostate-specific membrane antigen expression in metastatic differentiated thyroid cancer using 68Ga-HBED-CC-PSMA PET/CT. *Clin Nucl Med*. 2017;42:20–5.
- Lawhn-Heath C, Yom SS, Liu C, Villanueva-Meyer JE, Aslam M, Smith R, et al. Gallium-68 prostate-specific membrane antigen ([<sup>68</sup>Ga]Ga-PSMA-11) PET for imaging of thyroid cancer: a feasibility study. *EJNMMI Res*. 2020;10:128.
- Verma P, Malhotra G, Meshram V, Chandak A, Sonavane S, Lila AR, et al. Prostate-specific membrane antigen expression in patients with differentiated thyroid cancer with thyroglobulin elevation and negative iodine scintigraphy using 68Ga-PSMA-HBED-CC PET/CT. *Clin Nucl Med*. 2021;46:e406–9.
- Verma P, Malhotra G, Agrawal R, Sonavane S, Meshram V, Asopa RV. Evidence of prostate-specific membrane antigen expression in metastatic differentiated thyroid cancer using 68Ga-PSMA-HBED-CC PET/CT. *Clin Nucl Med*. 2018;43:e265–8.
- Santhanam P, Russell J, Rooper LM, Ladenson PW, Pomper MG, Rowe SP. The prostate-specific membrane antigen (PSMA)-targeted radiotracer 18F-DCFPyL detects tumor neovascularity in metastatic, advanced, radioiodine-refractory, differentiated thyroid cancer. *Med Oncol Northwood Lond Engl*. 2020;37:98.
- Wächter S, Di Fazio P, Maurer E, Manoharan J, Keber C, Pfestroff A, et al. Prostate-specific membrane antigen in anaplastic and poorly differentiated thyroid cancer—a new diagnostic and therapeutic target? *Cancers*. 2021;13:5688.
- Fugazzola L, Elisei R, Fuhrer D, Jarzab B, Leboulleux S, Newbold K, et al. 2019 European thyroid association guidelines for the treatment and follow-up of advanced radioiodine-refractory thyroid cancer. *Eur Thyroid J*. 2019;8:227–45.
- Brierly JD, Gospodarowicz MK, Wittekind C, editors. *TNM classification of malignant tumours*. 8th ed. Hoboken: Wiley; 2017.
- Kerseman K, De Man K, Courtyn J, Van Royen T, Piron S, Moerman L, et al. Automated radiosynthesis of Al[<sup>18</sup>F]PSMA-11 for large scale routine use. *Appl Radiat Isot Data Instrum Methods Use Agric Ind Med*. 2018;135:19–27.
- Boellaard R, Delgado-Bolton R, Oyen WJG, Giammarile F, Tatsch K, Eschner W, et al. FDG PET/CT: EANM procedure guidelines for tumour imaging: version 2.0. *Eur J Nucl Med Mol Imaging*. 2015;42:328–54.
- Xiao Z, Adam BL, Cazares LH, Clements MA, Davis JW, Schellhammer PF, et al. Quantitation of serum prostate-specific membrane antigen by a novel protein biochip immunoassay discriminates benign from malignant prostate disease. *Cancer Res*. 2001;61:6029–33.
- Bychkov A, Vutrpongwatana U, Tepmongkol S, Keelawat S. PSMA expression by microvasculature of thyroid tumors-potential implications for PSMA theranostics. *Sci Rep*. 2017;7:5202.
- Shi Y, Feng Y, Xu L, Li W, Guan L, Zuo R, et al. The value of gallium-68 prostate-specific membrane antigen ([<sup>68</sup>Ga]Ga-PSMA-11) PET/CT and 2-[<sup>18</sup>F]fluoro-2-deoxy-D-glucose (2-[<sup>18</sup>F]FDG) PET/CT in the detection of thyroid cancer lesions: a prospective head-to-head comparison. *Br J Radiol*. 2023;20230291.

41. Dietlein F, Kobe C, Neubauer S, Schmidt M, Stockter S, Fischer T, et al. PSA-stratified performance of 18F- and 68Ga-PSMA PET in patients with biochemical recurrence of prostate cancer. *J Nucl Med Off Publ Soc Nucl Med*. 2017;58:947–52.
42. Dietlein M, Kobe C, Kuhnert G, Stockter S, Fischer T, Schomäcker K, et al. Comparison of [18F]DCFPyL and [68Ga]Ga-PSMA-HBED-CC for PSMA-PET imaging in patients with relapsed prostate cancer. *Mol Imaging Biol*. 2015;17:575–84.
43. De Man K, Van Laeken N, Schelfhout V, Fendler WP, Lambert B, Kersemans K, et al. 18F-PSMA-11 versus 68Ga-PSMA-11 positron emission tomography/computed tomography for staging and biochemical recurrence of prostate cancer: a prospective double-blind randomised cross-over trial. *Eur Urol*. 2022;82:501–9.
44. Kuczynski EA, Reynolds AR. Vessel co-option and resistance to anti-angiogenic therapy. *Angiogenesis*. 2020;23:55–74.
45. Cuypers A, Truong A-CK, Becker LM, Saavedra-García P, Carmeliet P. Tumor vessel co-option: the past & the future. *Front Oncol*. 2022;12:965277.
46. Szabo V, Bugyik E, Dezso K, Ecker N, Nagy P, Timar J, et al. Mechanism of tumour vascularization in experimental lung metastases. *J Pathol*. 2015;235:384–96.
47. Bridgeman VL, Vermeulen PB, Foo S, Bilecz A, Daley F, Kostaras E, et al. Vessel co-option is common in human lung metastases and mediates resistance to anti-angiogenic therapy in preclinical lung metastasis models. *J Pathol*. 2017;241:362–74.
48. Schiffmann LM, Bruns CJ, Schmidt T. Resistance mechanisms of the metastatic tumor microenvironment to anti-angiogenic therapy. *Front Oncol*. 2022;12:897927.

## Publisher's Note

Springer Nature remains neutral with regard to jurisdictional claims in published maps and institutional affiliations.